Investigation into the Heterostructure Interface of CdSe-Based Core–Shell Quantum Dots Using Surface-Enhanced Raman Spectroscopy

Francesco Todescato,[†,*] Alessandro Minotto,[†] Raffaella Signorini,[†,*] Jacek J. Jasieniak,[‡] and Renato Bozio[†]

[†]Department of Chemical Science and U.R. INSTM, University of Padova, Via Marzolo 1, I-35131, Padova, Italy and [‡]Materials Science and Engineering, Ian Wark Laboratory, Commonwealth Scientific and Industrial Research Organization (CSIRO), Bayview Avenue, Clayton, 3168, Australia

ABSTRACT The structural nature of heterointerfaces in core–shell semiconductor quantum dots (QDs) plays a crucial role in tailoring their optical properties. In this work we have focused on using surface-enhanced Raman spectroscopy as a nondestructive tool to investigate the structural evolution of such interfaces in CdSe/CdS and CdSe/$Cd_{0.5}Zn_{0.5}S$ colloidal QDs. A comparison between the two systems shows significant structural variation across the core–shell interfaces for the two different materials: a smooth interface for the former and an abrupt interface for the latter. This structural difference modifies the electronic structure within the QDs, which directly dictates the confinement behavior of the electrons and holes. The implications of this translate to a better understanding of why graded CdSe/CdS/$Cd_{0.5}Zn_{0.5}S$/ZnS QDs are so lucrative for linear and nonlinear fluorescence-based applications.

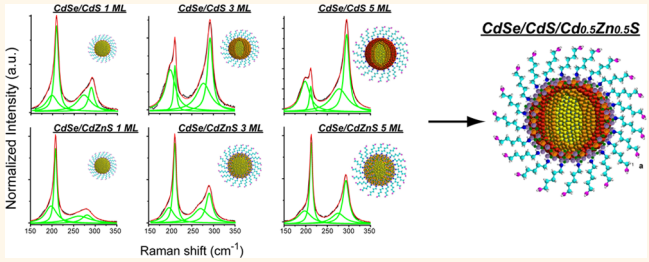

KEYWORDS: quantum dots · surface-enhanced resonant Raman spectroscopy · interface

The widespread interest in colloidal quantum dots (QDs) over the last three decades has largely stemmed from their lucrative light-emitting properties.[1−10] Through a gradual evolution in the understanding of how the surface of such nanocrystals can be overcoated with protective inorganic shells, photo- and chemically stable QDs can now be prepared with fluorescence quantum yields (FQY) reaching 100%.[11] Based largely on empirical observations, these advances have predominantly occurred for the archetypal CdSe core systems. The development of non-cadmium-based emitters with similar emission properties is a key milestone; however, it is clear that significant effort is required in first understanding exactly why CdSe-based core–shell structures possess such favorable fluorescence properties.

It is well known from the chemical vapor deposition community that lattice strain at interfaces results in nonepitaxial layer formation and consequently a defective interface.[12] Similar arguments have been made to account for the dependence of FQY on shell thickness.[13] In support of this structural picture, empirical experimental evidence from various core–shell structures has shown that the highest absolute quantum yields are achieved when minimal lattice strain exists at the core–shell interface.[14] Despite this, the structure of such interface remains largely unknown.

Recently, our group has demonstrated that epitaxially grown CdSe/CdS/$Cd_{0.5}Zn_{0.5}S$/ZnS QDs in solid-state matrixes present amplified spontaneous emission[15] and lasing[16,17] thresholds that are among the lowest for any reported QD system. The grading of the band gap in such nanocrystals localizes excitons away from the outer surface, in which traps responsible for nonradiative recombination are mainly localized.[18,19] Recent investigations into CdSe/CdS core–shell QDs by means of fluorescence line narrowing[20] and Raman spectroscopy[21] demonstrated that such "smoothing" is well satisfied by the CdSe/CdS QDs interface through the formation of an alloyed $CdSe_xS_{1-x}$ interlayer. This layer is found to gradually grow during shell

* Address correspondence to francesco.todescato@unipd.it; raffaella.signorini@unipd.it.

Received for review February 13, 2013 and accepted July 2, 2013.

Published online July 05, 2013
10.1021/nn402022z

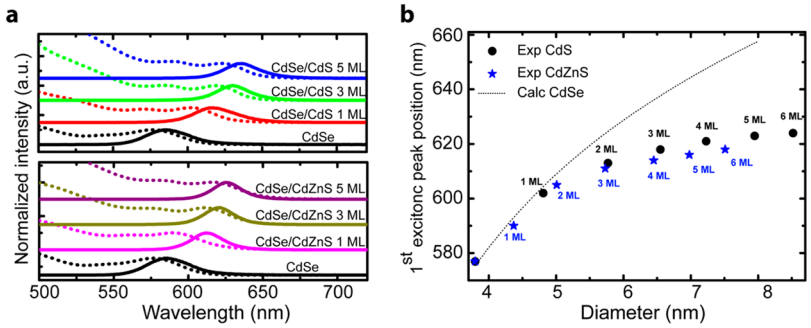

Figure 1. (a) Absorption (dotted lines) and emission (full lines) spectra of CdSe/CdS (upper panel) and CdSe/CdZnS core−shell QDs (lower panel) with different number of shell MLs (0, 1, 3, and 5). (b) First excitonic absorption peak position for CdSe cores (dotted line, evaluated using ref 27) and CdSe/CdS and CdSe/CdZnS (from 1 to 6 ML) QDs as a function of dot diameter.

formation up to a maximum of three CdS monolayers (MLs). As a result, the lattice structure is relaxed and the graded electronic levels create a smooth radial confinement potential. These factors enable inherently high FQYs in this system to be achieved, as well as advantageously enhance the optical gain lifetimes as a result of a reduced Auger recombination rate.[20,22]

The optimization of these two counteracting phenomena—the smoothing of the confinement potential and the exciton localization far from the outer surface—can be obtained using "giant" CdSe/CdS QDs with sizes as large as 15 nm.[23] In these nanocrystals (NCs) the trapping role of the external surface is avoided by its large distance from the CdSe core, and the potential smoothing is formed by the $CdSe_xS_{1-x}$ interfacial alloy. However, the use of such large nanocrystals for applications such as lasers is inherently challenging because of the difficulty to ensure colloidal stability in solution, while maintaining the required high volume fraction of emitters in a neat thin film or composite. An alternate nanocrystal heterostructure, which ultimately enables smaller QDs with high performances to be used, utilizes a radial material grading as recently theoretically proposed by Javaux *et al.*[19] This structure should provide an initial smoothing of the confinement potential and a gradual enhancement of the electronic barrier to prevent electron−hole migration toward the external surface.

The role of a $CdSe_xS_{1-x}$ alloy formed between CdSe/CdS QDs is well established. However, the use of CdS as a shell material presents a low potential barrier for electron migration. A more lucrative material would be one that possessed a higher confinement potential, but still permitted an adequate interfacial smoothing through alloy formation. The quest to find this material provides the motivation for the current work, wherein we study and compare the interface structure between CdSe cores and two shells, CdS (as a benchmark) and $Cd_{0.5}Zn_{0.5}S$ (henceforth CdZnS). CdZnS is a choice that allows a more strongly electronic confining potential with respect to CdS and can, in principle, partially preserve the smoothness of the confinement potential.

The interfacial lattice strain of CdS and CdZnS with respect to CdSe is predicted to be ∼4% and ∼8%, respectively.[14] By studying the interfaces for each core−shell structure as a function of shell thickness ranging from 1 to 6 MLs, we obtain an understanding of how variations in structural and electronic properties of the shell material influence the core−shell interface and the final optical properties of the NCs.

Raman spectroscopy is an important tool for the study of such interfaces. It has already been used to study Se/CdSe and ZnSe/CdSe multilayers,[24,25] CdTe/ZnTe heterojunctions,[26] and, as mentioned above, CdSe/CdS core−shell QDs at very low temperature (*i.e.*, 3 K).[21] In this work, we have opted to use surface-enhanced Raman spectroscopy (SERS). The main benefits of SERS in comparison to standard Raman spectroscopy are (i) the Raman signal is highly enhanced by the amplified near field of the plasma resonance close to the exciting laser and signal wavelengths and (ii) the metal presence quenches the residual fluorescence that can lower the quality of Raman spectra. As a result, a high signal-to-noise ratio is obtained with very small laser power (<50 μW), thus avoiding heating damage and allowing room-temperature (RT) measurements. The possibility to collect detailed Raman information at RT ensures the analysis of NCs with the same structural features, lattice dynamics, and optical properties present when the QDs are employed as emitters in photonic devices.

RESULTS AND DISCUSSION

In Figure 1a we show the evolution of the absorption features and the fluorescence band of CdSe/CdS and CdSe/CdZnS as a function of increasing number of shell monolayers. As expected, the first excitonic peak and the emission band of CdSe/CdS and CdSe/CdZnS core−shell QDs red-shift with increasing shell thickness. This behavior is commonly attributed to the difference in the energetic levels (and band gaps) between the three semiconductors (CdSe, CdS, CdZnS; see Supporting Information), which allow for partial delocalization of the exciton from the core to the shell.[23] Comparing the positions of the first excitonic

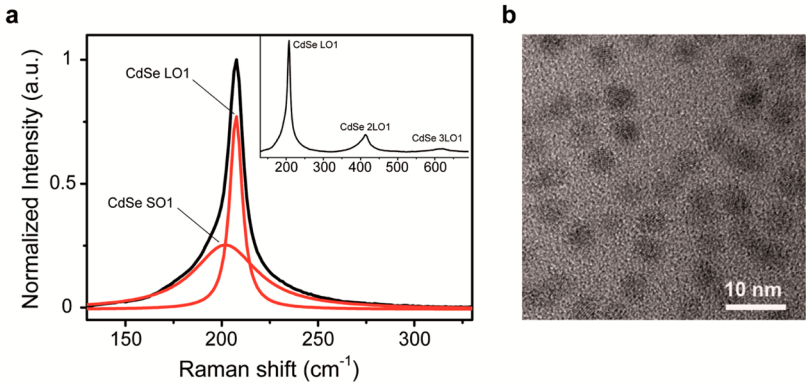

Figure 2. (a) Raman spectra of CdSe QDs with a diameter of 3.8 nm; (b) HR-TEM of CdSe QDs showing high sphericity and quality of cores.

peak of CdSe/CdS and of CdSe/CdZnS QDs with that of calculated homogeneous CdSe dots with the same overall size (Figure 1.b),[27] it is clear that the core−shell interface acts as a more stringent confinement barrier. Moreover, for the same ML number, the exciton confinement in the CdSe/CdZnS NCs is higher with respect to that in CdSe/CdS, with both shell types exhibiting saturation at approximately three shell MLs.

Naturally, the difference between pure CdSe cores and the core−shell QDs with the same size stems from the variation of the confinement potentials acting on the photogenerated electrons and holes. When comparing the two types of core−shell QDs, one must additionally take into account the different nature of the interface (abrupt, extended, *etc.*) arising from the changes in the lattice parameters and electronic features across the interface.

Quantum Dots on SERS Substrates. To study the bulk and interfacial properties of CdSe, CdSe/CdS, and CdSe/CdZnS QDs, we used surface-enhanced resonant Raman spectroscopy (SERRS, the 514 nm laser line employed is resonant with the interband transition for CdSe and CdS) coupled with the well-known silver film over nanosphere (FON) plasmonic substrates[28] (see Supporting Information). This particular substrate was chosen because of its high enhancement factor ($\geq 10^4$; see Methods), high thermal stability up to ~500 K (important for possible damages due to local laser heating during SERS experiments), high electrochemical stability, and long shelf life, >40 days.[29]

Despite the many advantages of SERS using an FON substrate, this geometry can alter the relative Raman band intensities due to the $1/r^{10}$ field enhancement dependence, r being the distance from the plasmonic surface.[30] In our studies, this problem should have a weak influence because the core−shell interface region is expected to be only up to ~1 nm thick (corresponding to approximately 3 MLs of shell). Moreover, considering that oleylamine is used as a capping agent, the QD surface is ~2 nm away from the substrate. This ensures that the core−shell interfaces of interest here are spatially located in a less steeply varying regime of the Raman ehancement.[30,31] Notably, for QDs with very large shells, the difference in the near-field enhancement factor can influence the relative longitudinal optical phonon intensity between core and shell materials. For this reason, our most relevant conclusions are based only on relative intensities from the narrow interface region.

SERRS of Pure CdSe Quantum Dots. CdSe QDs with a diameter of 3.8 nm have been used as cores for all of the core−shell NCs. For this reason, the first step before studying the more complicated core−shell systems is the analysis of the core features. In Figure 2a we show the Raman spectrum of the CdSe QDs (at room temperature) deposited on the FON substrate. The asymmetric band peaked at ~207 cm^{-1} is a convolution of two peaks. The fitting with Lorentzian functions identifies two modes: the principal one, centered at 207.7 cm^{-1}, which is the first-order longitudinal optical phonon of CdSe (LO1); and a second mode, centered at 201.7 cm^{-1}, which originates from the CdSe surface optical phonon modes (SO1).[32−34] Two overtones of the longitudinal optical phonon are also observed around 410 cm^{-1} (2LO1) and 615 cm^{-1} (3LO1) (Figure 2a, inset).

The differences between the Raman features of CdSe QDs and bulk CdSe (LO1 asymmetry, higher fwhm, and different peak position with respect to the 213 cm^{-1} band of the bulk[35]) can be attributed to the spatial confinement of phonons in NCs and, in particular, to the relaxation of the $q = 0$ selection rule.[36] Because of the high sphericity of the core NCs (Figure 2b), it is possible to calculate the theoretical peak position of the CdSe QDs with a diameter of 3.8 nm by exploiting the phonon confinement model (PCM) using a Gaussian confinement function.[37] Following this model, our LO1 mode should be peaked at 208.7 cm^{-1}, in good agreement with our experimental value (Figure 3). The PCM and experimental value differ by 1 cm^{-1}, which can be ascribed to the surface tension present on the dot surface. The compressive stress on

our NC surface, evaluated using the Laplace relation,[38] is about 0.67 GPa. When this is considered in accordance with the Grüneisen differential relationship, this gives rise to a shift of the LO1 band by about 1 cm^{-1}.[35] The final difference between the experimental and the PCM LO1 position falls well below our instrumental resolution (~1 cm^{-1}; see Methods).

SERRS of CdSe/CdS Quantum Dots. As far as we know, in Figure 4a–c are presented for the first time SERRS spectra of CdSe/CdS QDs as a function of shell thickness at room temperature, which accounts for all the possible changes of conduction bands[19] from low temperature used in previous studies.[21] Each spectrum shows prominent Raman bands centered at ~209 cm^{-1} (A band) and 290 cm^{-1} (B band). As for the CdSe QDs, the A band is a convolution of two peaks, the longitudinal optical CdSe phonon mode (LO1) centered at ~209 cm^{-1} (A1 band) and a surface optical phonon mode (SO1) centered at ~200 cm^{-1} (A2 band). A comparison of the integrated intensities of both bands provides insight into the variation of the bulk to surface structure. The integral of the A2 band strongly increases with increasing shell thickness and exceeds the contribution of the A1 band above 3 CdS MLs (Figure 4b, Figure 5, and Table 1). For larger shell thicknesses, the integral of the A2 band saturates (Table 1). This behavior suggests that not only is such a band due to surface optical phonon modes, but there is also an additional contribution due to the formation of a $CdSe_xS_{1-x}$ alloy that radially extends out by ~1 nm (*i.e.*, 3 CdS MLs) from the core, as already described by Tschirner *et al.*[21] and Garcia-Santamaria *et al.*[20] Conceivably, the alloy formation must involve anionic interfacial diffusion from within the CdSe core.[20,39] This is verified by the lowering of the A1 band area up to 3 MLs of CdS before saturation. The deconvolution of the A2 band (as the B2 band, *vide infra*) is not possible because Raman bands at RT are intrinsically larger with respect to those measured at liquid helium temperature.[21]

The alloy formation is further confirmed by analyzing the second Raman feature peaked at 290 cm^{-1}. This B band also exhibits two main contributions: a longitudinal optical phonon mode originating from CdS, centered at ~290 cm^{-1} (B1 band), and a second peak at ~275 cm^{-1} (B2 band). The latter peak is composed of two contributions: the surface optical phonon modes of CdS[40] and the interfacial alloy layer formed between the CdSe core and CdS shell.[20,21,41]

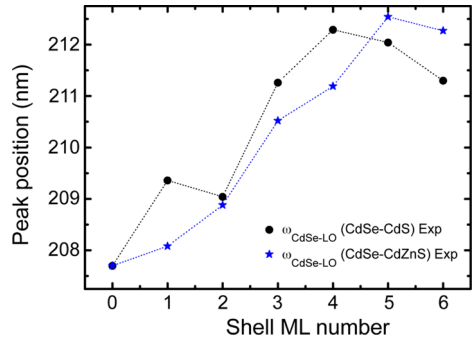

Figure 3. Longitudinal optical phonon band position for CdSe in CdSe/CdS and CdSe/CdZnS QDs as a function of shell MLs (lines are just guides for the eyes). From the peak position shift it is possible to evaluate $\Delta c/c$ for CdSe cores due to the growth of shell multilayers. The point at 0 ML refers to core CdSe (*i.e.*, QDs with a diameter of 3.8 nm).

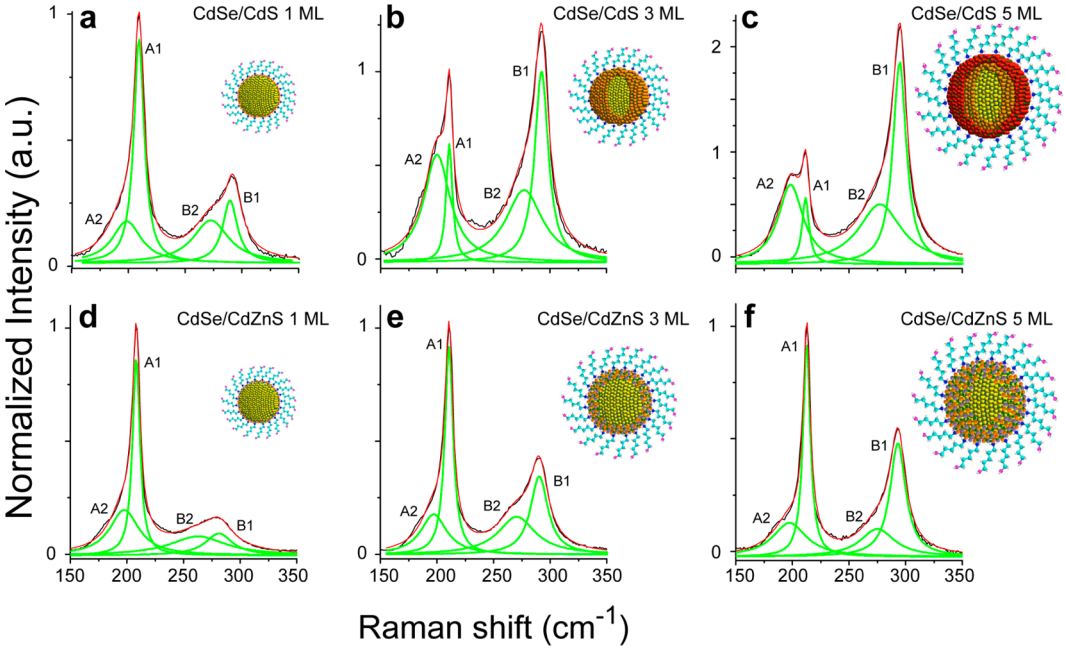

Figure 4. SERRS spectra of CdSe and CdS-like bands for different numbers of ML of CdSe/CdS and CdSe/CdZnS QDs. All spectra are normalized to the maximum of the A band (note the relative *y*-axes). In the insets, schematic representations of CdSe/CdS and CdSe/CdZnS QDs with different shell ML numbers are reported.

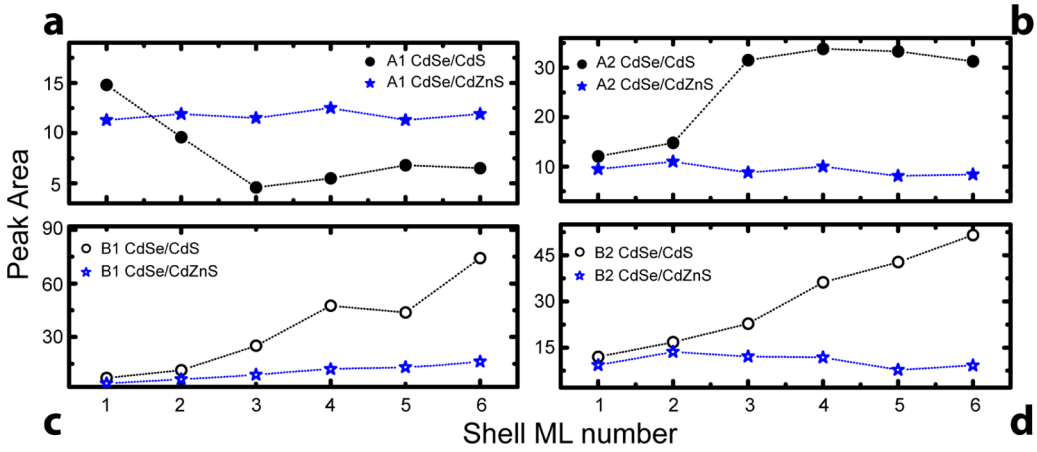

Figure 5. (a) Longitudinal CdSe (A1) phonon band area for CdSe/CdS and CdSe/CdZnS QDs; (b) CdSe (A2) phonon band area for CdSe/CdS and CdSe/CdZnS QDs; (c) longitudinal CdS (B1) phonon band area for CdSe/CdS and CdSe/CdZnS QDs; (d) CdS (B2) phonon band area for CdSe/CdS and CdSe/CdZnS QDs. In all spectra, lines are just guides for the eyes.

TABLE 1. QDs Overall Diameter (*d*, nm), Experimental CdSe and CdS LO Phonon Frequencies (in cm^{-1}), and Related Lattice Parameter Variation, $\Delta c/c$[51,52a]

MLs	*d* (nm)	A1 (cm^{-1})	$\Delta c/c$ CdSe (%)[b]	A1 area	A2 area	B1 (cm^{-1})	$\Delta c/c$ CdS (%)[b]	B1 area	B2 area
1	4.81	208.4	−0.10	14.8 ± 0.9	12.1 ± 1.1	290.4	0.98	7.1 ± 0.9	12.0 ± 1.2
2	5.77	209.0	−0.19	9.6 ± 0.8	14.8 ± 2.3	289.2	1.09	11.4 ± 2.0	16.8 ± 6.5
3	6.55	211.3	−0.51	4.6 ± 1.5	31.5 ± 5.1	292.9	0.77	25.1 ± 2.4	22.8 ± 6.5
4	7.23	212.3	−0.66	5.5 ± 2.5	33.8 ± 8.7	294.5	0.64	47.5 ± 5.9	36.2 ± 5.4
5	7.95	212.0	−0.62	6.8 ± 1.0	33.3 ± 3.4	294.9	0.61	43.7 ± 1.9	42.8 ± 2.6
6	8.52	211.3	−0.52	6.5 ± 0.7	31.3 ± 1.7	295.8	0.53	74.2 ± 7.8	51.6 ± 3.7

[a] The relative band areas of all the LO and SO Raman features for CdSe/CdS QDs with shells from 1 to 6 MLs are also reported. [b] Negative and positive values mean compressive and tensile strain, respectively .

As expected, the integrated areas of B1 and B2 bands continuously increase with increasing CdS shell thickness (Figure 4a−c and Table 1). A comparison of the A1 and B1 peak frequencies shows a gradual blue-shift with increased shell growth. This behavior is associated with the variation of the bond length in the CdSe and CdS lattices as caused by interfacial lattice strain. X-ray diffraction (XRD) measurements confirm this finding.[21] The variation of the lattice parameter[34] in lattice-strained QDs can be evaluated employing the Grüneisen equation.[42,43] The outcomes of this analysis for different CdS MLs are reported in Table 1 ($\Delta c/c$ values) and are consistent with previous results on CdSe/CdS NCs.[21] The lattice parameter of CdSe is about 4% higher with respect to the CdS one. Such a difference in lattice constant leads to a compressive strain (negative $\Delta c/c$ values) in the core and a tensile one in the shell (positive $\Delta c/c$ values), responsible for the aforementioned lattice parameter variation.

SERRS of CdSe/CdZnS Quantum Dots. In Figure 4d−f we show the SERRS spectra of CdSe/CdZnS as a function of shell thickness. Analogous to that for CdSe/CdS, we observe Raman bands centered at ∼208 cm^{-1} (A band) and ∼290 cm^{-1} (B band). The deconvolution of each band with two Lorentzian functions confirms again the existence of the CdSe longitudinal optical phonon band at ∼208 cm^{-1} (A1 band) and a CdS-"like" longitudinal optical phonon mode at ∼290 cm^{-1} (B1 band). The appearance of this latter contribution has been already reported for CdSe/ZnS QDs.[39,41] It was attributed to the formation of a mixed CdZnS(Se) alloy layer.[44] In our case, the CdS-"like" signal is due to the presence of CdS in the shell composition. As is shown in Table 2, the integrated areas of the B1 bands exhibit a slight increase with increasing shell thickness. This is consistent with a gradual increase in the Cd−S bond concentration during the shell growth. Meanwhile, the A1, A2, and B2 bands remain almost constant during shell growth (Figure 5). This indicates that, unlike for CdS shells, interdiffusion between the CdSe core and the CdZnS shell is confined to the first shell ML (∼0.3 nm).

The abrupt nature of the CdSe/CdZnS interface must induce significant stress across the nanocrystals. To better appreciate this, we utilized an analogous analysis to that for CdSe/CdS to determine the extent of lattice parameter variation by comparing the frequencies of the A1 and B1 bands (Table 2). This analysis shows that the CdZnS shell induces strain on the nanocrystals that modifies its bond length, a conclusion that is confirmed by XRD measurements (see Supporting Information). Interestingly, the extent of

TABLE 2. QDs Overall Diameter (*d*, nm), Experimental CdSe and $Cd_{0.5}Zn_{0.5}S$ LO Phonon Frequencies (in cm^{-1}), and Related Lattice Parameter Variation, $\Delta c/c$[a]

MLs	*d* (nm)	A1 (cm^{-1})	$\Delta c/c$ CdSe (%)[b]	A1 area	A2 area	B1 (cm^{-1})	$\Delta c/c$ CdS[c] (%)[b]	B1 area	B2 area
1	4.37	208.1	−0.06	11.3 ± 0.5	9.5 ± 0.4	281.2	1.80	4.0 ± 0.8	9.3 ± 1.0
2	5.01	208.9	−0.17	11.9 ± 0.4	11.0 ± 0.4	286.8	1.29	6.3 ± 0.1	13.6 ± 1.4
3	5.73	210.5	−0.41	11.5 ± 1.2	8.8 ± 1.6	290.3	0.99	8.9 ± 0.9	12.1 ± 1.0
4	6.45	211.2	−0.50	12.5 ± 0.4	10.0 ± 0.6	292.0	0.85	12.0 ± 0.4	11.8 ± 1.6
5	6.98	212.5	−0.69	11.3 ± 0.3	8.1 ± 0.8	293.2	0.75	13.1 ± 0.3	7.8 ± 1.2
6	7.51	212.3	−0.65	11.9 ± 0.4	8.4 ± 1.0	294.1	0.67	16.2 ± 1.2	9.2 ± 1.1

[a] The relative band areas of all the LO and SO Raman features for CdSe/CdS QDs with shells from 1 to 6 MLs are also reported. [b] Negative and positive values mean compressive and tensile strain, respectively. [c] CdS-"like" band, see SERRS of CdSe/CdZnS Quantum Dots section.

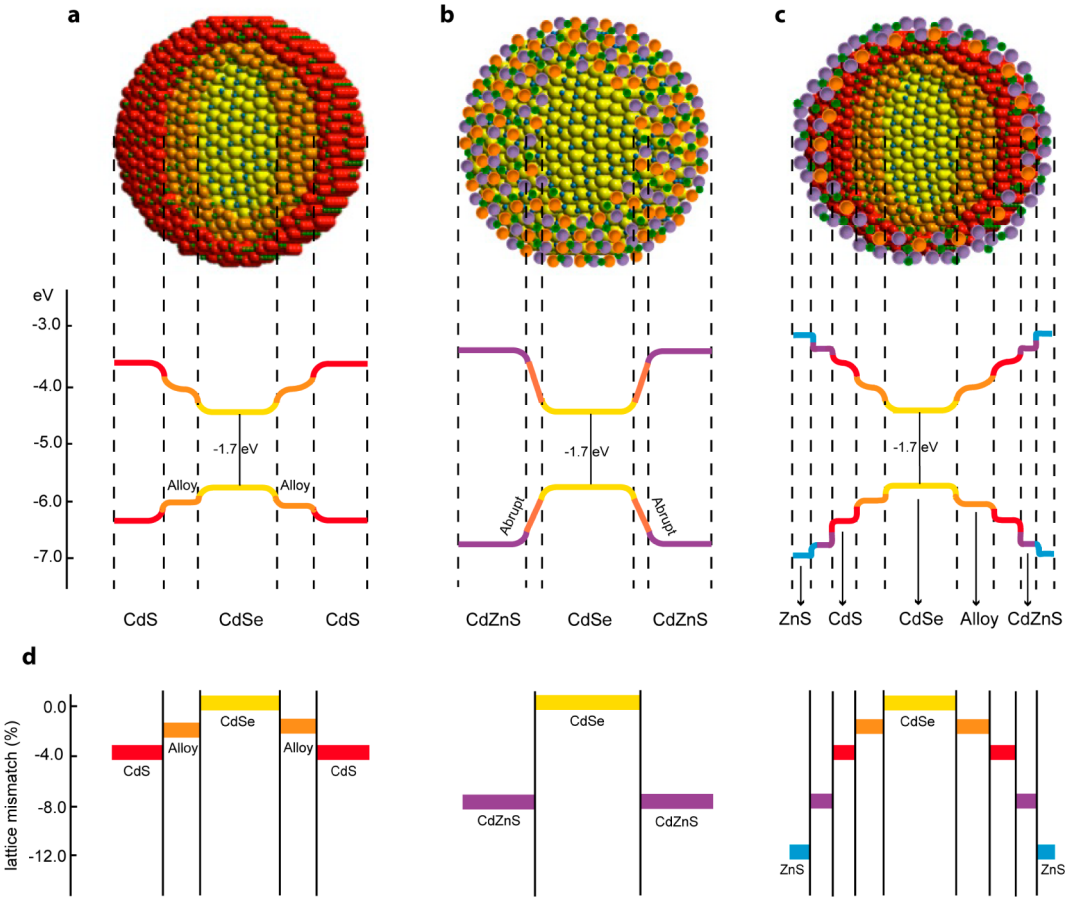

Figure 6. Schematic structure of CdSe/CdS (a), CdSe/CdZnS (b), and CdSe/CdS/CdZnS/ZnS graded QDs with the respective material bulk energy levels (as reported in ref 14). The orange intermixed layer in the CdSe/CdS (and CdSe/CdS/CdZnS/ZnS) structure represents the $CdSe_xS_{1-x}$ alloy formation. (d) Lattice mismatch differences between the materials employed in the QDs (ref 14).

stress in the nanocrystals appears to level off after ~5 MLs of growth. In comparison, the stress is relieved within ~3 MLs in CdSe/CdS. This suggests that for CdSe/CdS QDs the stress for the core is relived more effectively with respect to CdSe/CdZnS. This is probably due to the lattice mismatch difference between the two shell materials. The observed $CdSe_xS_{1-x}$ alloy formation, with the associated increase of the lattice parameter, further contributes to the stress relief.

Alloying of CdSe/ZnSe core−shell nanocrystals to form CdZnSe nanocrystals has been previously reported.[45] The transition temperature to induce this behavior was found to be in excess of 270 °C. For the CdZnS case, because of the same ions involved (and the comparable average lattice parameters of CdZnS and ZnSe[46]), one may expect similar temperatures for an efficient ion diffusion. For the synthesis of our CdSe/CdZnS nanocrystals, the growth temperature was limited to 250 °C (see Supporting Information). Notably, from our experience, this is practically the maximum growth temperature to achieve high-quality core−shell nanocrystals. The experimental results show that

for QDs obtained with our synthetic route the temperature is insufficient to allow the ions to diffuse for any significant interfacial alloying to occur. A direct outcome of this finding is that CdZnS cannot be used directly as a material to smooth the confinement potential because it forms an abrupt interface with CdSe.

Perspective on Optimizing Core/Shell QDs. A defect-free, epitaxially grown shell is instrumental to achieving high fluorescence yields in core–shell QDs. In addition to these linear optical properties, Cragg and Efros[22] have reported that "smoothing out" the confinement potential in NCs results in a reduction of 3 orders of magnitude for the Auger recombination rate. Such "smoothing" is well satisfied by $CdSe_xS_{1-x}$ alloy formation in CdSe/CdS QDs. However, for thin shell thicknesses, it also enables sufficient electron and hole delocalization toward the outer surface, which is plagued by surface traps that reduce fluorescence yields.[18,19] To overcome this problem, "giant" nanocrystals have been grown, but, as aforementioned, such large QDs may present problems. The attempt to directly use $Cd_{0.5}Zn_{0.5}S$ (that presents a stronger electronic confining potential with respect of CdS) to obtain smaller QDs does not allow preserving the smoothing of the confinement potential.

The key to obtain small and performing QDs with a smoothed confinement potential resided in the mitigation of exciton delocalization in CdS using a $Cd_{0.5}Zn_{0.5}S$ overlayer, which gives a graded shell composition framed by subsequent higher band gap materials, thus strongly confining excitons away from the defective outer surface, as proposed by Javaux *et al.*[19] This rationalization likely explains the origin of the extremely high FQYs and the low amplified spontaneous emission[15] and lasing[16,17] thresholds observed for CdSe/CdS/$Cd_{0.5}Zn_{0.5}S$/ZnS QDs, where a final ML of ZnS is sufficient to provide a last "electronic" barrier against electron–hole delocalization and ultimately to improve the chemical stability (Figure 6).

CONCLUSION

We have employed for the first time surface-enhanced Raman spectroscopy as a tool to study the core–shell interface of CdSe/CdS and CdSe/$Cd_{0.5}Zn_{0.5}S$ QDs at room temperature. For both core–shell systems the longitudinal optical phonon peaks provided insight into the interface formation between the different materials in the QDs. CdSe/CdS QDs were found to exhibit alloy formation with a radial extension of ~1 nm (*i.e.*, 3 MLs). In the CdSe/$Cd_{0.5}Zn_{0.5}S$ case an abrupt interface limited to ~0.3 nm (*i.e.*, 1 ML) was observed. The structural and electronic variations across these interfaces have enabled a more complete understanding of both types of core–shell nanocrystals. In addition they have shown that if the design principle for efficient QDs is to engineer a gradual increase of the potential barrier up to a value that effectively prevents the carrier from reaching the NC surface, still keeping their dimension to a minimum, a natural solution would be as follows: proceed by growing a graded shell ML by ML with a gradual change of composition, starting at CdS and ending at ZnS.

This concept gives a good explanation of why CdSe/CdS/$Cd_{0.5}Zn_{0.5}S$/ZnS QDs is a nearly ideal nanocrystal heterostructure for use in visible-range luminescence and optically pumped lasing applications. Importantly, this study demonstrates that by applying similar concepts to that outlined here, a scientific roadmap can be envisaged for optimizing the interfacial structure of any core–shell QDs, a huge step forward from the empirically derived optimization currently employed.

METHODS

QDs Synthesis. CdSe cores were prepared following a slightly modified method described by van Embden *et al.*[47] Core–shell quantum dots were prepared according to a modified SILAR protocol that has been previously published.[48] Briefly, washed CdSe cores were dispersed in a 1:1 mixture of oleylamine (70% purity, Aldrich)/1-octadecene (90% Aldrich) at a concentration of 40 μM. Following degassing at RT for 30 min, the solution was slowly heated to 80 °C under vacuum. The atmosphere was changed to N_2, and the degassed solution was heated to 235 °C. At this point a Cd enriching layer was added, which was the equivalent to a half stoichiometric ML of CdSe. After 5 min, an equivalent quantity of ODE-S was added to form 1 ML of shell material. This was allowed to grow for 10 min prior to the addition of an equivalent amount of Cd or CdZn stock solution. After 15 min the solution temperature was reduced to 120 °C to take aliquots of the samples after each ML. The temperature was then increased to a value of between 235 and 250 °C. The exact final temperature was increased by 5 °C every 2 MLs up to a maximum of 250 °C. As synthesized core–shell QDs were purified through multiple extractions using MeOH, EtOH, and acetone, prior to being dispersed in toluene.

The sulfur stock solution used during shell formation consisted of sulfur (>99.5%, Aldrich) dissolved in 1-octadecene at a concentration of 1 M at 150 °C for 1 h. The metal precursor stocks were prepared by dissolving cadmium or 1:1 cadmium/zinc acetate hydrate salts (>98%, Aldrich) in 1-octadecene using a 7:1 excess of oleic acid (Aldrich)/bis(2,2,4-trimethylpentyl)-phosphinic acid (Cytec Specialty Chemicals) at 280 °C for 1 h. The final metal concentration was 1 M.

SERS Samples. To obtain film over nanosphere substrates, 2.5 × 2.5 cm^2 glass slides were cleaned first in acid piranha solution (H_2SO_4/H_2O_2 = 3:1) at ~80 °C for 1 h and then sonicated in basic piranha solution ($NH_4OH(30\%)/H_2O_2$ = 5:1) for 1 h. The substrates were cleaned numerous times and kept in deionized water. Before using, the slides were dried using a N_2 flux. Then 100 μL of 1% polystyrene nanosphere solution (Fisher Scientific, with 150 nm diameter) in water was spin-coated on top of the glass slides to form a self-assembled mask. Finally Ag thin films were deposited onto the substrates in an Edwards E306A coating system with a bare pressure of 6×10^{-5} mbar. The metal deposition rate was ~1 Å/s, and the final Ag thickness, evaluated by means of a quartz crystal microbalance, was about 150 nm. Finally, 30 μL of QDs solutions was spun on top of the FON substrates at 500 rpm for 1 min.

Optical Characterizations. The UV–visible absorption spectra were recorded using a Cary 5 spectrometer (Varian) in the range

350−800 nm. The fluorescence spectra were measured with a FluoroMax P (Jobin-Yvon) fluorimeter in the 500−750 nm range exciting at 490 nm with a xenon lamp.

SERS Measurements. SERS measurements were performed with a micro-Raman instrument, employing a 50× microscope objective (NA = 0.75). Samples were excited with a 514 nm wavelength line of an Ar^+ gas laser. The Raman signals are collected with a nitrogen-cooled CCD and present a resolution of ~1 cm^{-1}. To evaluate the enhancement factor (EF), the silver nanostructures were functionalized with benzenthiol (BT) by dipping each sample in a solution of 25 L of BT in 25 mL of methanol for about 20 h. Then samples were rinsed repeatedly in methanol, and the EF was obtained using the equation[49]

$$EF = \frac{I^{Raman,\,Monolayer}}{I^{Raman,\,Liquid}} \frac{C_v H_{eff}}{C_s} \frac{\sigma_{Toluene}}{\sigma_{BT}}$$

where σ_{BT} is the BT differential cross section, $\sigma_{Toluene}$ is the toluene differential cross section, and their ratio was directly measured, C_v is the toluene volumetric density (5.69×10^{21} molecules/cm^3), C_s is the BT packing density on the surface (6.8×10^{14} molecules/cm^2),[45] and H_{eff} is the collection efficiency dependent on the collection apparatus and on the effective scattering volume of the sample.

For SERS measurements the laser power on the sample surface is kept lower than ≤50 μW to avoid any possible laser damage on the QD structure or FON substrates.

An evaluation of the temperature on the substrate is obtaining exploiting Stokes and anti-Stokes Raman signals, giving a temperature of about 154 ± 38 °C. Under resonance SERS conditions, the anti-Stokes/Stokes ratio can give only an approximate estimate of the sample temperatures for a number of reasons: different resonance conditions and plasmon enhancement affect differently Stokes and anti-Stokes spectra, and differences of the coupling of excitons with different phonon modes may yield off-equilibrium phonon distributions.[50] The CCD detector was calibrated using the optical longitudinal phonon of silicon, centered at 520 cm^{-1}.

Experimental data reported in Table 1 and Table 2 are mean values of many different measurements. Each spectrum was recorded as an average of 10 spectra, each one collected with an integration time of 10 s.

Conflict of Interest: The authors declare no competing financial interest.

Acknowledgment. Acknowledgments are due to PRAT_2010 project prot. CPDA104332/10 of University of Padova and PRIN prot. 2009YSP28A. F.T. acknowledges "Assegno di Ricerca Senior" Repertorio 76-2012 of University of Padova. J.J. acknowledges the Australian Research Council for support through the APD grant DP110105341. The authors are grateful also to Prof. C. Ferrante for stimulating discussions, to Prof. Brusatin for XRD measurements, and to Prof. Mattei for the CdSe size distribution analysis.

Supporting Information Available: Bulk energy level scheme of semiconductor materials. CdSe/CdS and CdSe/CdZnS diameters and relative excitonic peak position. Scannig electron microscopy image of film over nanosphere plasmonic substrate. TEM and XRD of CdSe/CdZnS core−shell QDs. This information is available free of charge *via* the Internet at http://pubs.acs.org.

REFERENCES AND NOTES

1. Rogach, A. *Semiconductor Nanocrystal Quantum Dots: Synthesis, Assembly, Spectroscopy and Application*; Springer: Berlin, 2008.
2. Zhao, J.; Zhang, J.; Jiang, C.; Bohnenberger, J.; Basché, T.; Mews, A. Electroluminescence from Isolated CdSe/ZnS Quantum Dots in Multilayered Light-Emitting Diodes. *J. Appl. Phys.* **2004**, *96*, 3206–3210.
3. Coe, S.; Woo, W.-K.; Bawendi, M.; Bulovic, V. Electroluminescence from Single Monolayers of Nanocrystals in Molecular Organic Devices. *Nature* **2002**, *420*, 800–803.
4. Mews, A.; Zhao, J. Light-Emitting Diodes: A Bright Outlook for Quantum Dots. *Nat. Photonics* **2007**, *1*, 683–684.
5. Wang, C.; Wehrenberg, B. L.; Woo, C. Y.; Guyot-Sionnest, P. Light Emission and Amplification in Charged CdSe Quantum Dots. *J. Phys. Chem. B* **2004**, *108*, 9027–9031.
6. Schaller, R. D.; Petruska, M. A.; Klimov, V. I. Tunable Near-Infrared Optical Gain and Amplified Spontaneous Emission Using PbSe Nanocrystals. *J. Phys. Chem. B* **2003**, *107*, 13765–13768.
7. Eisler, H. J.; Sundar, V. C.; Bawendi, M. G.; Walsh, M.; Smith, H. I.; Klimov, V. Color-Selective Semiconductor Nanocrystal Laser. *Appl. Phys. Lett.* **2002**, *80*, 4614–4616.
8. Malko, A. V.; Mikhailovsky, A. A.; Petruska, M. A.; Hollingsworth, J. A.; Htoon, H.; Bawendi, M. G.; Klimov, V. I. From Amplified Spontaneous Emission to Microring Lasing Using Nanocrystal Quantum Dot Solids. *Appl. Phys. Lett.* **2002**, *81*, 1303–1305.
9. Achermann, M.; Petruska, M. A.; Koleske, D. D.; Crawford, M. H.; Klimov, V. I. Nanocrystal-Based Light-Emitting Diodes Utilizing High-Efficiency Nonradiative Energy Transfer for Color Conversion. *Nano Lett.* **2006**, *6*, 1396–1400.
10. Schaller, R. D.; Agranovich, V. M.; Klimov, V. I. High-Efficiency Carrier Multiplication through Direct Photogeneration of Multi-Excitons *via* Virtual Single-Exciton States. *Nat. Phys.* **2005**, *1*, 189–194.
11. Greytak, A. B.; Allen, P. M.; Liu, W.; Zhao, J.; Young, E. R.; Popovic, Z.; Walker, B. J.; Nocera, D. G.; Bawendi, M. G. Alternating Layer Addition Approach to CdSe/CdS Core/Shell Quantum Dots with Near-Unity Quantum Yield and High On-Time Fractions. *Chem. Sci.* **2012**, *3*, 2028–2034.
12. Davies, J. H. *The Physics of Low-Dimensional Semiconductors*; Cambridge University Press, 1998.
13. Dabbousi, B. O.; Rodriguez-Viejo, J.; Mikulec, F. V.; Heine, J. R.; Mattoussi, H.; Ober, R.; Jensen, K. F.; Bawendi, M. G. (CdSe)ZnS Core-Shell Quantum Dots: Synthesis and Characterization of a Size Series of Highly Luminescent Nanocrystallites. *J. Phys. Chem. B* **1997**, *101*, 9463–9475.
14. Xie, R.; Kolb, U.; Li, J.; Basché, T.; Mews, A. Synthesis and Characterization of Highly Luminescent CdSe-Core CdS/$Zn_{0.5}Cd_{0.5}S$/ZnS Multishell Nanocrystals. *J. Am. Chem. Soc.* **2005**, *127*, 7480–7488.
15. Todescato, F.; Fortunati, I.; Gardin, S.; Garbin, E.; Collini, E.; Bozio, R.; Jasieniak, J. J.; Della Giustina, G.; Brusatin, G.; Toffanin, S.; *et al.* Soft-Lithographed Up-Converted Distributed Feedback Visible Lasers Based on CdSe−CdZnS−ZnS Quantum Dots. *Adv. Funct. Mater.* **2012**, *22*, 337–344.
16. Signorini, R.; Fortunati, I.; Todescato, F.; Gardin, S.; Bozio, R.; Jasieniak, J. J.; Martucci, A.; Della Giustina, G.; Brusatin, G.; Guglielmi, M. Facile Production of Up-Converted Quantum Dot Lasers. *Nanoscale* **2011**, *3*, 4109–4113.
17. Xing, G.; Liao, Y.; Wu, X.; Chakrabortty, S.; Liu, X.; Yeow, E. K. L.; Chan, Y.; Sum, T. C. Ultralow-Threshold Two-Photon Pumped Amplified Spontaneous Emission and Lasing from Seeded CdSe/CdS Nanorod Heterostructures. *ACS Nano* **2012**, *6*, 10835–10844.
18. Klimov, V. I. Spectral and Dynamical Properties of Multiexcitons in Semiconductor Nanocrystals. *Annu. Rev. Phys. Chem.* **2007**, *58*, 635–673.
19. Javaux, C.; Mahler, B.; Dubertret, B.; Shabaev, A.; Rodina, A. V.; Efros, Al. L.; Yakovlev, D. R.; Liu, F.; Bayer, M.; Camps, G.; *et al.* Thermal Activation of Non-Radiative Auger Recombination in Charged Colloidal Nanocystals. *Nat. Nanotechnol.* **2013**, *8*, 206–212.
20. Garcia-Santamaria, F.; Brovelli, S.; Viswanatha, R.; Hollingsworth, J. A.; Htoon, H.; Crooker, S. A.; Klimov, V. I. Breakdown of Volume Scaling in Auger Recombination in CdSe/CdS Heteronanocrystals: The Role of the Core−Shell Interface. *Nano Lett.* **2011**, *11*, 687–693.
21. Tschirner, N.; Lange, H.; Schliwa, A.; Biermann, A.; Thomsen, C.; Lambert, K.; Gomes, R.; Hens, Z. Interfacial Alloying in CdSe/CdS Heteronanocrystals: A Raman Spectroscopy Analysis. *Chem. Mater.* **2012**, *24*, 311–318.
22. Cragg, G. E.; Efros, A. L. Suppression of Auger Processes in Confined Structures. *Nano Lett.* **2010**, *10*, 313–317.
23. Garcia-Santamaria, F.; Chen, Y.; Vela, J.; Schaller, R. D.; Hollingsworth, J. A.; Klimov, V. I. Suppressed Auger

Recombination in "Giant" Nanocrystals Boosts Optical Gain Performance. *Nano Lett.* **2009**, *9*, 3482–3488.
24. Nesheva, D.; Kotsalas, I.; Raptis, C.; Vateva, E. On the Structural Stability of Amorphous Se/CdSe Multilayers: a Raman Study. *J. Non-Cryst. Solids* **1998**, *224*, 283–290.
25. Nesheva, D.; Raptis, C.; Levi, Z.; Bineva, I.; Aneva, Z. Alloying at the Interface of ZnSe/CdSe Multilayers and ZnSe-CdSe Composite Films: A Raman Study. *Asian J. Phys.* **2000**, *9*, 289–298.
26. Zielony, E.; Placzek-Popko, E.; Henrykowski, A.; Gumienny, Z.; Kamyczek, P.; Jacak, J.; Nowakowski, P.; Karczewski, G. Laser Irradiation Effects on the CdTe/ZnTe Quantum Dot Structure Studied by Raman and AFM Spectroscopy. *J. Appl. Phys.* **2012**, *112*, 063520.
27. Jasieniak, J.; Smith, L.; van Embden, J.; Mulvaney, P.; Califano, M. Re-examination of the Size-Dependent Absorption Properties of CdSe Quantum Dots. *J. Phys. Chem. C* **2009**, *113*, 19468–19474.
28. Van Duyne, R. P.; Hulteen, J. C.; Treichel, D. A. Atomic Force Microscopy and Surface-Enhanced Raman Spectroscopy. I. Ag Island Films and Ag Film over Polymer Nanosphere Surfaces Supported on Glass. *J. Chem. Phys.* **1993**, *99*, 2101–2114.
29. Dieringer, J. A.; McFarland, A. D.; Shah, N. C.; Stuart, D. A.; Whitney, A. V.; Yonzon, C. R.; Young, M. A.; Zhang, X.; Van Duyne, R. P. Surface Enhanced Raman Spectroscopy: New Materials, Concepts, Characterization Tools, and Applications. *Faraday Discuss.* **2006**, *132*, 9–26.
30. Stiles, P. L.; Dieringer, J. A.; Shah, N. C.; Van Duyne, R. P. Surface-Enhanced Raman Spectroscopy. *Annu. Rev. Anal. Chem.* **2008**, *1*, 601–626.
31. Kennedy, B. J.; Spaeth, S.; Dickey, M.; Carron, K. T. Determination of the Distance Dependence and Experimental Effects for Modified SERS Substrates Based on Self-Assembled Monolayers Formed Using Alkanethiols. *J. Phys. Chem. B* **1999**, *103*, 3640–3646.
32. Comas, F.; Studarta, N.; Marquesa, G. E. Optical Phonons in Semiconductor Quantum Rods. *Solid State Commun.* **2004**, *130*, 477–480.
33. Lange, H.; Artemyev, M.; Woggon, U.; Thomsen, C. Geometry Dependence of the Phonon Modes in CdSe Nanorods. *Nanotechnology* **2009**, *20*, 045705.
34. Trallero-Giner, C.; Debernardi, A.; Cardona, M.; Menéndez-Proupín, E.; Ekimov, A. I. Optical Vibrons in CdSe Dots and Dispersion Relation of the Bulk Material. *Phys. Rev. B* **1998**, *57*, 4664–4669.
35. Meulemberg, R. W.; Jennings, T.; Strouse, G. F. Compressive and Tensile Stress in Colloidal CdSe Semiconductor Quantum Dots. *Phys. Rev. B* **2004**, *70*, 235311.
36. Richter, H.; Wang, Z. P.; Ley, L. The One Phonon Raman Spectrum in Microcrystalline Silicon. *Solid State Commun.* **1981**, 625–629.
37. Campbell, I. H.; Fauchet, P. M. The Effects of Microcrystal Size and Shape on the Phonon Raman Spectra of Crystalline Semiconductors. *Solid State Commun.* **1986**, *58*, 739–741.
38. Szleifer, I.; Kramer, D.; Ben-Shaul, A.; Gelbart, W. M.; Safran, S. A. Molecular Theory of Curvature Elasticity in Surfactant Films. *J. Chem. Phys.* **1990**, *92*, 6800–6817.
39. Dzhagan, V. M.; Valakh, M. Y.; Raevskaya, A. E.; Stroyuk, A. L.; Kuchmiy, S. Y.; Zahn, D. R. T. Characterization of Semiconductor Core−Shell Nanoparticles by Resonant Raman Scattering and Photoluminescence Spectroscopy. *Appl. Surf. Sci.* **2008**, *255*, 725–727.
40. Lu, L.; Xu, X. L.; Liang, W. T.; Lu, H. F. 406221 Raman Analysis of CdSe/CdS Core−Shell Quantum Dots with Different CdS Shell Thickness. *J. Phys.: Condens. Matter* **2007**, *19*, 406221.
41. Dzhagan, V. M.; Valakh, M. Y.; Raevska, O. E.; Stroyuk, O. L.; Kuchmiy, S. Y.; Zahn, D. R. T. The Influence of Shell Parameters on Phonons in Core−Shell Nanoparticles: A Resonant Raman Study. *Nanotechnology* **2009**, *20*, 365704.
42. Alivisatos, A. P.; Harris, T. D.; Brus, L. E.; Jayaraman, A. Resonance Raman Scattering and Optical Absorption Studies of CdSe Microclusters at High Pressure. *J. Chem. Phys.* **1988**, *89*, 5979–5982.
43. Scamarcio, G.; Lugara, M.; Manno, D. Size-Dependent Lattice Contraction in $CdS_{1-x}Se_x$ Nanocrystals Embedded in Glass Observed by Raman Scattering. *Phys. Rev. B* **1992**, *45*, 13792–13795.
44. Dzhagan, V. M.; Valakh, M. Y.; Raevskaya, A. E.; Stroyuk, A. L.; Kuchmiy, S. Y.; Zahn, D. R. T. Resonant Raman Scattering Study of CdSe Nanocrystals Passivated with CdS and ZnS. *Nanotechnology* **2007**, *18*, 285701.
45. Zhong, X.; Han, M.; Dong, Z.; White, T. J.; Knoll, W. Composition-Tunable $Zn_xCd_{1-x}Se$ Nanocrystals with High Luminescence and Stability. *J. Am. Chem. Soc.* **2003**, *125*, 8589–8594.
46. Lide, D. R. *Handbook of Chemistry and Physics*, 84th ed.; CRC Press, 2004.
47. van Embden, J.; Mulvaney, P. Nucleation and Growth of CdSe Nanocrystals in a Binary Ligand System. *Langmuir* **2005**, *21*, 10226–10233.
48. van Embden, J.; Jasieniak, J.; Mulavaney, P. Mapping the Optical Properties of CdSe/CdS Heterostructrue Nanocrystals: The Effect of Core Size and Shell Thickness. *J. Am. Chem. Soc.* **2009**, *131*, 14299–14309.
49. Le Ru, E. C.; Blackie, E.; Meyer, M.; Etchegoin, P. G. Surface Enhanced Raman Scattering Enhancement Factors: A Comprehensive Study. *J. Phys. Chem. C* **2007**, *111*, 13794–13803.
50. Itoh, T.; Yoshida, K.; Biju, V.; Kikkawa, Y.; Ishikawa, M.; Ozaki, Y. Second Enhancement in Surface-Enhanced Resonance Raman Scattering Revealed by an Analysis of Anti-Stokes and Stokes Raman Spectra. *Phys. Rev. B* **2007**, *76*, 085405.
51. Hwang, Y. N.; Shin, S.; Park, H. L.; Park, S. H.; Kim, U.; Jeong, H. K.; Shin, E. J.; Kim, D. Effect of Lattice Contraction on the Raman Shifts of CdSe Quantum Dots in Glass Matrices. *Phys. Rev. B* **1996**, *54*, 15120–15124.
52. Zhang, J. Y.; Wang, X. Y.; Xiao, M.; Qu, L.; Peng, X. Lattice Contraction in Free-Standing CdSe Nanocrystals. *Appl. Phys. Lett.* **2002**, *81*, 2076–2077.